Centralized Control of Distributed Single-Phase Inverters Arbitrarily Connected to Three-Phase Four-Wire Microgrids

Danilo I. Brandao, *Member, IEEE*, Tommaso Caldognetto, *Member, IEEE*, Fernando P. Marafão, *Member, IEEE*, Marcelo G. Simões, *Fellow, IEEE*, José A. Pomilio, *Senior Member, IEEE*, and Paolo Tenti, *Fellow, IEEE*

Abstract—This paper proposes an effective technique to control the power flow among different phases of a three-phase four-wire distribution power system by means of single-phase converters arbitrarily connected among the phases. The aim is to enhance the power quality at the point-of-common-coupling of a microgrid, improve voltage profile through the lines, and reduce the overall distribution losses. The technique is based on a master/slave organization where the distributed single-phase converters act as slave units driven by a centralized master controller. Active, reactive, and unbalance power terms are processed by the master controller and shared proportionally among distributed energy resources to achieve the compensation target at the point-of-common-coupling. The proposed control technique is evaluated in simulation considering the model of a real urban power distribution grid under non-sinusoidal and asymmetrical voltage conditions. The main results, concerning both steady-state and transient conditions, are finally reported and discussed.

Index Terms—Line-interactive inverter, master/slave control, microgrid, power flow control, unbalance compensation.

I. Introduction

THE CONSISTENT increase of energy needs and the relevant concerns with environmental impacts are propelling the diffusion of distributed energy resources (DERs) based on renewable energy [1]. In particular, the significant penetration of DERs and a wider adoption of information and communication technologies (ICT) in low-voltage grids indicate a gradual evolution toward the microgrid concept [2], [3]. Apart from that, the transition to a more efficient and sustainable power system brings several technical challenges; typical examples are: control of active and reactive power sharing among resources, ensure reliable operation under different grid conditions (e.g., weak-grid, distorted grid voltage, frequency variations), manage overproduction, coordinate distributed intelligent systems [4], coordinate power sharing among phases [5], minimize operational costs.

In this scenario, three-phase AC power systems represent a solid basis to support DERs integration and the development of the microgrid concept [6], facilitating power exchange among microgrids while taking advantage of the existing distribution network infrastructure. On the other hand, different distribution power system topologies are adopted around the world: a) three-phase three-wire, b) three-phase three-wire with grounded neutral, c) three-phase four-wire with non-grounded neutral, d) three-phase four-wire with grounded neutral and contiguous ground [7]. If we also consider how loads are actually connected in each country, the scenario gets even more intricate, because single-phase devices can be either connected line-to-neutral or line-to-line. From the standpoint of microgrid control the connection code is extremely relevant, particularly for compensation purposes.

In three-phase systems, load balancing is a critical issue and, at the same time, an inherent need of electrical distribution systems [8]. Indeed, load unbalances may cause detrimental effects, like voltage asymmetry and increased distribution losses. A direct solution, viable especially for newly designed microgrids, is to fix the connection code of the loads; however, this may be unfeasible in most existing distribution systems. Employing compensators for voltage asymmetry can be another solution [9], though it involves additional costs. Whereas, exploiting the surplus power capability of DERs to compensate unbalance power has been proven to be a good solution, not requiring additional investments [8], [10]. In [11] and [12], unbalance compensation were proposed through three-phase inverters, whereas in [13], an unbalance power compensation by means of single-phase inverters exclusively connected line-to-neutral to a three-phase network is proposed. However, managing inverters arbitrarily connected (i.e., line-to-neutral or line-to-line) to three-phase networks, in order to control the power flow among different phases, has not been addressed so far.

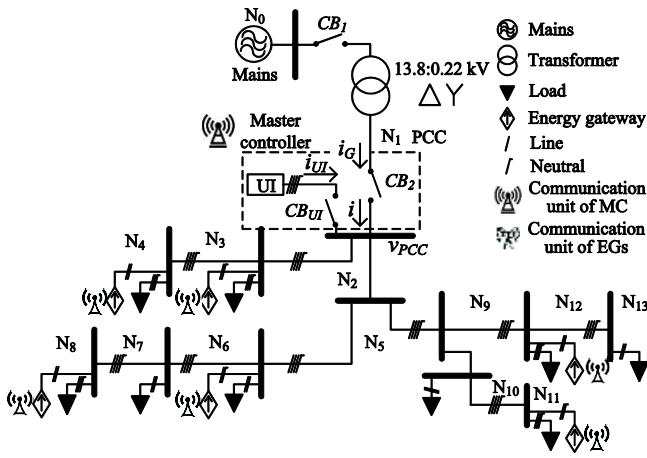In this context, this paper proposes an effective technique to control the power flow among different phases of three-phase

Fig. 1. Considered three-phase four-wire microgrid structure with line-to-neutral and line-to-line connected DERs and loads.

Fig. 2. Equivalent circuit of the system in Fig. 1, with the required polarity scheme for line-to-neutral and line-to-line connected inverters.

four-wire microgrids by means of single-phase converters arbitrarily connected among the phases. The proposed technique requires neither the knowledge of line impedance parameters nor the use of current phasor measurements [8]. The aim is to enhance the power quality measured at the point-of-common-coupling (PCC) of the microgrid with the main grid, to improve the voltage profile through the lines and to reduce the overall distribution losses while preserving an efficient operation of DERs.

II. MICROGRID STRUCTURE

To introduce the proposed control algorithm, let us consider the microgrid structure shown in Fig. 1. It employs a master/slave control architecture, where the *master controller* (MC) is located at the microgrid PCC (N_1) and drives a set of slave units, called *energy gateways* (EGs), by suitable power commands sent through an ICT infrastructure. The EGs are electronic power processors (EPP) that interface DERs (e.g., renewable sources, storage devices) to the microgrid. The MC drives also a grid-interactive inverter installed at PCC, called *utility interface* (UI), which refines the microgrid operation seen from the mains (N_0) and meets temporary energy needs to ensure fault ride-through capability and soft transitions from and to the islanded operation [14].

Before proceeding with further details on the structure of the microgrid, we should define with the notation $EG_{mn\text{Nj}}$ a generic EG connected at the *j*-th node (N_j) of the distribution network among phases *m* and *n*, namely, the phase *a*, phase *b*, phase *c*, or neutral conductor of the network. Therefore, for example, $EG_{ab\text{N4}}$ indicates a particular EG connected at the fourth node (N_4) between phase *a* and phase *b*, while $EG_{crm\text{N6}}$ indicates an EG connected at the sixth node (N_6) between phase *c* and neutral conductor. We underline that the measured quantities in an EG are the current through the EPP and the voltage across its points of connection, following the Fig. 2 polarities.

For what concerns the structure of the particular low-voltage microgrid of Fig. 1, it consists in fourteen nodes, nine distinct loads, and six single-phase EGs, of which three are connected
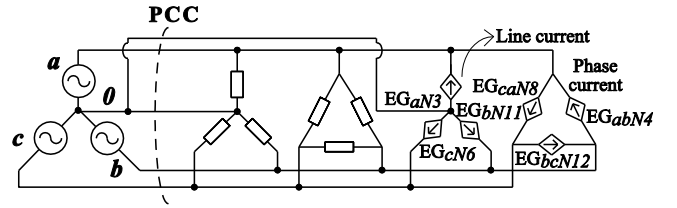
line-to-neutral ($EG_{a\text{N3}}$, $EG_{b\text{N11}}$, $EG_{c\text{N6}}$) and three are connected line-to-line ($EG_{ab\text{N4}}$, $EG_{bc\text{N12}}$, $EG_{ca\text{N8}}$). All the EGs are controlled as *current sources* synchronized with the fundamental grid voltage. The passive nodes (i.e., those nodes with no EGs connected) may host linear and nonlinear loads, and are generally not equipped with smart meters. The UI is a three-phase grid-interactive inverter equipped with energy storage (e.g., battery, super-cap) installed at the microgrid PCC. The UI is always controlled as a *voltage source* and, in general, it performs as a grid-supporting voltage source during grid-connected operation and as a grid-forming voltage source during islanded operation [15]. A communication infrastructure is assumed to provide the narrowband communication link between MC and distributed EGs that is needed to implement the coordinated control by the power-based algorithm [16]. It is worth remarking that the use of communication is limited to microgrid's optimization functions; if communication failures occur, the basic functions of DERs, as well as all the functions that can be performed autonomously, keep on operating normally.

The control architecture is hierarchically organized in three layers. The primary (*local*) control layer manages the basic and specific functions, such as: local energy management, local compensation of reactive and harmonic currents generated by the local loads, and local voltage stabilization. The secondary control layer, whose implementation is *distributed* among MC and EGs, manages the active and reactive power sharing among EGs with the aim of regulating the overall power absorption by exploiting every available DER in an efficient manner. The tertiary (*global*) control layer manages the interaction between the whole microgrid and the mains [17]. In practice, the hierarchical control architecture is prioritized, which means that EGs obey the MC commands as long as the local constraints are met; for example as shown in [18], in which a local controller acts independently of MC if the local voltages transcend predefined ranges.

Although the line-to-line connection scheme is not generally accepted, it is a common practice in some regions of South America, especially in Brazil, even for residential consumers. Fig. 2 shows the equivalent three-phase four-wire circuit corresponding to the scheme of Fig. 1. From Fig. 2, it is clear to realize that the current flowing through the single-phase DER units, from the MC point of view, is *line current* for line-to-neutral connected inverters or *phase current* for line-to-line connected inverters.

An advantage of line-to-line connected DERs is the reduced current exchange through their corresponding EPPs, thanks to

the higher voltage value across their points of connection. On the other hand, by standing on only two phases, the line-to-line inverters are decoupled from the neutral wire, which prevents neutral (i.e., homopolar) current compensation.

III. BASICS OF CPT

The Conservative Power Theory (CPT) [19] is used to assess the microgrid power status and to generate the MC power commands to the slave units (i.e., EGs). The CPT offers a meaningful and computationally efficient approach to manage power quantities referring to different grid nodes, even in presence of asymmetrical and distorted voltage [20]. Being based on conservative power quantities, the approach is not affected by voltage and phase shift caused, for example, by transformers, or by harmonic distortion in grid voltages and currents [20].

CPT is a natural frame (*abc*) based power theory, valid for any voltage and current waveform and applicable to single- and poly-phase systems. It proposes a decomposition of power and current quantities in their subcomponents, which are associated to distinct physical electrical characteristics, such as: average active power transfer, reactive energy, load unbalance power, and distortion power.

Preliminarily, to introduce the fundamental notation of CPT [19], let us consider a generic poly-phase circuit under periodic operation. In the following, instantaneous and RMS quantities are denoted with lowercase and uppercase symbols, respectively, and vector quantities (i.e., collective values)[1] with boldface symbols.

The three-phase *active power* is defined by the product:

$$P = \frac{1}{T} \cdot \sum_{m=1}^{M} \int_0^T v_m(t) \cdot i_m(t) dt, \tag{1}$$

where T is the line voltage fundamental period and m indicates phase variables. According to the CPT, the three-phase *reactive energy* is defined by:

$$W = \frac{1}{T} \cdot \sum_{m=1}^{M} \int_0^T \hat{v}_m(t) \cdot i_m(t) dt, \tag{2}$$

where $\hat{v}_m$ is the unbiased voltage integral, namely, the integral of phase voltage v_m minus its average value. Multiplying W by the line voltage fundamental angular frequency (ω) the *reactive power* $Q = \omega \cdot W$ is obtained.

The CPT is based on the orthogonal decomposition of the instantaneous phase current (i_m) into decoupled terms:

$$i_m = i_{am}^b + i_{rm}^b + i_{am}^u + i_{rm}^u + i_{vm} = i_{am}^b + i_{nam}, \tag{3}$$

such that i^b_a is the balanced active current, i^b_r is the balanced reactive current, i^u_a is the unbalanced active current, i^u_r is the unbalanced reactive current, i_v is the void current, and i_{na} is the non-active current.

The *balanced active currents* are defined as the minimum RMS currents needed to convey the total active power. By using (1), these currents are given by:

$$i_{am}^b = \frac{P}{V^2} \cdot v_m = G^b \cdot v_m, \tag{4}$$

where G^b is the *equivalent balanced conductance*. Similarly, the *balanced reactive currents* are defined as the minimum RMS currents needed to convey the total reactive energy. By using (2), these currents are given by:

$$i_{rm}^b = \frac{W}{\widehat{V}^2} \cdot \hat{v}_m = B^b \cdot \hat{v}_m, \tag{5}$$

where B^b is the *equivalent balanced reactivity*. Note that B^b is in some sense dual to the concept of G^b.

If the load is balanced, the PCC absorbs only balanced active and reactive currents; otherwise, it drains also *unbalance currents*, which are defined by:

$$i_m^u = \left(G_m - G^b\right) \cdot v_m + \left(B_m - B^b\right) \cdot \hat{v}_m = i_{am}^u + i_{rm}^u, \tag{6}$$

$$G_m = \frac{P_m}{V_m^2} \; ; \;\; G^b = \frac{P}{V^2} \;\; and \;\; B_m = \frac{W_m}{\hat{V}_m^2} \; ; \;\; B^b = \frac{W}{\widehat{V}^2}, \tag{7}$$

such that G_m and B_m are the *equivalent phase conductance* and *reactivity*, respectively, and, i^u_m is the unbalanced currents. Note that if the system is balanced the *equivalent phase conductance* is equal to the *equivalent balanced conductance* (i.e., $G_m = G^b$). Similarly, the reactivity parameters are equal (i.e., $B_m = B^b$).

Finally, the *void currents* are defined as the remaining phase currents. These represent all the load nonlinearity currents (i.e., distortions):

$$i_{vm} = i_m - i_{am}^b - i_{rm}^b - i_m^u. \tag{8}$$

Since all the previous current terms are orthogonal to each other, the collective RMS current can be calculated as:

$$I^2 = I_a^{b2} + I_r^{b2} + I^{u2} + I_v^2 = I_a^{b2} + I_{na}^2. \tag{9}$$

Accordingly, multiplying the collective RMS current and voltage, the apparent power (A) can also be split as:

$$A^2 = V^2 \cdot I^2 = P^2 + Q^2 + N^2 + D^2, \tag{10}$$

such that:
- P is the active power and corresponds to the real power converted into work;
- Q is the reactive power and reveals the presence of reactive energy in linear inductors and capacitors, or even a fundamental phase shift caused by nonlinear loads (e.g., thyristor rectifiers);
- N is the unbalance power, equal to $\sqrt{N_a^2 + N_r^2}$, where N_a is caused by unbalanced loads with resistive characteristic (elements that do not cause fundamental phase shift) and N_r is caused by unbalanced loads with non-resistive characteristic (elements that cause fundamental phase shift);
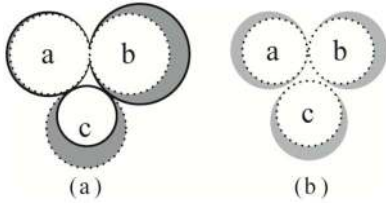- D is the distortion power and it is related to load nonlinearities.

Fig. 3. Representation of unbalance compensation. The figure indicates: equivalent phase parameter (solid line circles), equivalent balanced parameter (dotted line circles), difference between phase and balanced parameters (dark grey areas), and uniform power generation (light grey areas).

Note that only the active power and the reactive energy are conservative quantities regardless of the voltage condition.

IV. UNBALANCED CURRENT COMPENSATION CONCEPT

Let us consider Fig. 3 to explain the concept of the distributed compensation of the unbalance currents with imbalance EGs contributions among the phases. The unbalanced active currents compensation and, subsequently, the unbalanced reactive compensation are explained here.

Assuming the area of each solid line circle to represent the *equivalent phase conductance* (G_m), which corresponds to the amount of active power absorbed at phase m within the microgrid (P_{Lm}). In Fig. 3.a, solid line circles have different areas, indicating an unbalanced system ($G_a \neq G_b \neq G_c$) [19]. Solid areas are split into two parts: the circles surrounded by dotted line, with equal areas for all the phases, representing the *equivalent balanced conductance* (G^b), and the dark grey areas, with different dimensions, representing the difference between the *equivalent phase conductance* and the *equivalent balanced conductance* of a particular phase [G_m-G^b, as in (6)]. The sum of the areas enclosed by dotted lines is the total three-phase active power absorbed in the microgrid [$P_{Lt} = P$, as in (1)].

According to the CPT [19], a balanced system must consist in only *equivalent balanced conductance* (G^b), which corresponds to only dotted line circles in Fig. 3. Then, to compensate the unbalance and attain a balanced system ($G_m = G^b$), it is needed to minimize the dark grey area of Fig. 3.a. One can note now, that the dark grey areas are different among the phases, resulting in an imbalance contribution of the EGs among the phases. Secondly, the balance is always ensured by the EGs if their power capacities are not limited, as in Fig. 3.b. Of course, under limited capability only a partial balancing of the system is achieved by means of the EGs, leaving the remainder to the UI.

The same concept is applied to unbalanced reactive currents compensation by using the *equivalent phase reactivity* (B_m) and *equivalent balanced reactivity* (B^b). Note that the unbalanced active currents compensation is enabled by the EGs that are equipped with energy storage devices, which give them the flexibility of delivering or storing active power. However, the effectiveness of the unbalanced reactive currents compensation does not rely on the storage device, because it handles only reactive power.

V. POWER FLOW CONTROL IN THREE-PHASE FOUR-WIRE MICROGRIDS BY MEANS OF POWER-BASED CONTROL

The power-based control was initially proposed in [16] to drive EGs so that they contribute to microgrid power needs in proportion of their actual capability to deliver active and reactive power. This approach achieves the regulation of the power flow at the PCC by using a couple of coefficients (α_P, α_Q). These coefficients, herein called *scaling coefficients*, are broadcasted to all the EGs and are meant to scale the power contributions from EGs, so that DERs are uniformly exploited in contributing to the whole microgrid's power needs, with minimal communication and measurement requirements.

Recently, in [13], the power-based control was adapted to perform unbalance currents compensation, considering only line-to-neutral connections for the inverters. To this end, the power-based control algorithm is applied independently to each phase-m of the three-phase microgrid, and a couple of scaling coefficients—called, in this case, *phase scaling coefficients* (α_{Pm}, α_{Qm})—were calculated and broadcasted to all the EGs connected to that phase.

This section extends the application of the power-based control to include power flow control among different phases and to perform the unbalance currents compensation by means of single-phase inverters arbitrarily connected to a three-phase four-wire distribution network.

Briefly, the control operation consists of the following steps. At the beginning of each control cycle (which lasts few periods of line voltage) the MC polls each EG connected to the microgrid. Then, the EGs return the actual amount of active and reactive power currently delivered to the grid and their residual power capacity that can be shared for the benefit of the microgrid. Finally, on the basis of received data, measured energy exchange at PCC, and negotiation with the distribution system operator (DSO), the MC computes the power contribution requested to EGs for the next cycle.

It is worth recalling that each EG must inform the MC of the particular phase at which it is connected. For an EG connected between phases "m" and "n", it is sufficient to inform only about the phase "m", following the adopted polarities of Fig. 2, and measured voltage v_{mn}, as explained in Section II. Moreover, new DERs can be any time connected to the grid by sending a request to the MC, which therefore must update the list of the microgrid's EGs per phase.

Next, the power-based control is considered to develop the unbalance current compensation concept described in Section IV and the power flow control described above.

A. Power-Based Control Algorithm Per Phase

More specifically, the coordinated control strategy performs as follows. At the end of the l-th control cycle, the MC determines the total *per phase* active power $P^*_{Gmt}(l)$ and reactive power $Q^*_{Gmt}(l)$ that must be shared among EGs along that cycle. Moreover, the j-th EG ($j = 1, 2, \ldots, J$) sends the following information to MC:

- its active power $P_{Gj}(l)$ and reactive power $Q_{Gj}(l)$ generated during the l-th control cycle;

- the minimum active power $P_{Gj}^{min}(l)$ and the maximum active power $P_{Gj}^{max}(l)$ that the EG can generate, on the basis of the state of its energy storage, if any;
- the nominal apparent power $A_{Gj}(l)$ of the local EPP and its overload apparent power $A_{Gj}^{over}(l)$ (i.e., the maximum apparent power the EG can generate for a limited period of time).

On the basis of the collected data, MC calculates:

- the total active and reactive phase power delivered by the EGs along cycle *l*:

$$P_{Gmt}(l) = \sum_{j=1}^{J} P_{Gmj}(l), \qquad (11.a)$$

$$Q_{Gmt}(l) = \sum_{j=1}^{J} Q_{Gmj}(l), \qquad (11.b)$$

and, in the same way, the total minimum $[P_{Gmt}^{min}(l)]$ and maximum $[P_{Gmt}^{max}(l)]$ active phase power and total maximum $[Q_{Gmt}^{max}(l)]$ and overloading $[Q_{Gmt}^{over}(l)]$ reactive phase power; to that end, the maximum deliverable reactive power and the overload reactive power of the *j*-th EG are computed as:

$$Q_{Gj}^{max}(l) = \sqrt{A_{Gj}(l)^2 - P_{Gj}(l)^2}, \qquad (12.a)$$

$$Q_{Gj}^{over}(l) = \sqrt{A_{Gj}^{over}(l)^2 - P_{Gj}(l)^2}. \qquad (12.b)$$

The overload condition operates during a limited period of time, based on the thermal-stress of EPP, and it communicates with the MC through A_{Gj}^{over} variable.

- the total active and reactive phase power absorbed within the microgrid during cycle *l*:

$$P_{Lmt}(l) = P_{Gridm}(l) + P_{UIm}(l) + P_{Gmt}(l), \quad (13.a)$$
$$Q_{Lmt}(l) = Q_{Gridm}(l) + Q_{UIm}(l) + Q_{Gmt}(l), \quad (13.b)$$

where P_{Gridm} and Q_{Gridm} are the active and reactive phase power measured at the PCC's grid side, and P_{UIm} and Q_{UIm} are the active and reactive phase power delivered by UI;

- the references for the total active $[P^*{}_{Gmt}(l+1)]$ and reactive $[Q^*{}_{Gmt}(l+1)]$ phase power to be provided by the EGs in the next control cycle *l+1*:

$$P_{Gmt}^*(l+1) = P_{Lmt}(l) - P_{PCCm}^*(l+1), \quad (14.a)$$
$$Q_{Gmt}^*(l+1) = Q_{Lmt}(l) - Q_{PCCm}^*(l+1), \quad (14.b)$$

where $P^*{}_{PCCm}(l+1)$ and $Q^*{}_{PCCm}(l+1)$ are, respectively, the active and reactive references of the phase power flow at the PCC. These references are set by MC to regulate the power flow at the PCC among different phases, according to the energy state of the UI and EGs (see [21]). They are estimated, for the next control cycle, on the basis of the quantities measured during the last control cycle. Considering the polarities of Fig. 1, the exchanged powers at the terminals of the UI are:

$$P_{UIm}(l+1) = P_{PCCm}^*(l+1) - P_{Gridm}^*(l+1), \quad (15.a)$$
$$Q_{UIm}(l+1) = Q_{PCCm}^*(l+1) - Q_{Gridm}^*(l+1). \quad (15.b)$$

TABLE I
PHASE SCALING COEFFICIENTS

Power condition	Scaling coefficients
$P_{Gmt}^*(l+1) < P_{Gmt}^{min}(l)$	$\alpha_{Pm} = 0$
$P_{Gmt}^{min}(l) \le P_{Gmt}^*(l+1) < P_{Gmt}(l)$	$\alpha_{Pm} = \dfrac{P_{Gmt}^*(l+1) - P_{Gmt}^{min}(l)}{P_{Gmt}(l) - P_{Gmt}^{min}(l)}$
$P_{Gmt}(l) \le P_{Gmt}^*(l+1) \le P_{Gmt}^{max}(l)$	$\alpha_{Pm} = 1 + \dfrac{P_{Gmt}^*(l+1) - P_{Gmt}(l)}{P_{Gmt}^{max}(l) - P_{Gmt}(l)}$
$P_{Gmt}^*(l+1) > P_{Gmt}^{max}(l)$	$\alpha_{Pm} = 2$
$Q_{Gmt}^*(l+1) \le Q_{Gmt}^{max}(l)$	$\alpha_{Qm} = \dfrac{Q_{Gmt}^*(l+1)}{Q_{Gmt}^{max}(l)}$
$Q_{Gmt}^*(l+1) > Q_{Gmt}^{max}(l)$	$\alpha_{Qm} = 1 + \dfrac{Q_{Gmt}^*(l+1) - Q_{Gmt}^{max}(l)}{Q_{Gmt}^{over}(l) - Q_{Gmt}^{max}(l)}$

Grid power references P^*_{Gridm} and Q^*_{Gridm} guarantee the balanced condition at the grid side, and they are set on the basis of long term energy management strategies (e.g., negotiations with the DSO) or set to zero in islanded mode.

- finally, the *phase scaling coefficients* α_{Pm} and α_{Qm} (both ranging in the interval [0, 2]) are computed and broadcasted to all the EGs connected to the corresponding phase *m*. The active power is controlled by variable α_{Pm}, while the reactive power is controlled by variable α_{Qm}. Table I reports the calculation of these coefficients for different conditions.

Thus, given α_{Pm} and α_{Qm}, the *j*-th EG (EG$_j$) controls its local active and reactive power injection according to:

$$P_{Gj}^*(l+1) = P_{Gj}^{min} + \left(P_{Gj} - P_{Gj}^{min}\right) \cdot min(\alpha_{Pm}, 1)$$
$$+ \left(P_{Gj}^{max} - P_{Gj}\right) \cdot max(\alpha_{Pm} - 1, 0), \qquad (16.a)$$
$$Q_{Gj}^*(l+1) = Q_{Gj}^{max} \cdot min(\alpha_{Qm}, 1)$$
$$+ \left(Q_{Gj}^{over} - Q_{Gj}^{max}\right) \cdot max(\alpha_{Qm} - 1, 0), \quad (16.b)$$

where $P^*{}_{Gj}(l+1)$ and $Q^*{}_{Gj}(l+1)$ are respectively the active and reactive power references for EG$_j$ in the next control cycle. Equations (16) hold for the control of the power flow at PCC, in both grid-connected and islanded operation.

Summarizing, considering the EGs connected to phase *m*:

- *active power:* i) if $\alpha_{Pm} = 0$, the EGs supply their minimum power; ii) if $0 = \alpha_{Pm} < 1$, the EGs ensure the power balance by operating in reduced power mode [22], or diverting the excess of generated power to distributed storage units, if any; iii) if $1 = \alpha_{Pm} < 2$, the EGs meet the microgrid power demand by drawing energy from energy storage devices; iv) if $\alpha_{Pm} = 2$, all EGs connected to phase *m* supply the maximum power.
- *reactive power:* i) if $0 = \alpha_{Qm} < 1$, the EGs compensate the reactive power; ii) if $1 = \alpha_{Qm} < 2$ the reactive compensation is attained by temporarily overloading the EGs.

In every operating condition the power balance must be ensured by exploiting the UI, by readjusting loads/generators or, in grid-connected mode, by taking power from the mains.

Therefore, the unbalance current compensation concept described in Section IV can be attained by employing the

TABLE II
PARAMETERS OF THE THREE-PHASE FOUR-WIRE
LOW-VOLTAGE MICROGRID

Distorted and asymmetrical voltages [kV] at node N_0		
$V_a = 11.84 \cdot \sin(\omega t) + 0.34 \cdot \sin(3 \cdot \omega t) +$ $+0.34 \cdot \sin(5 \cdot \omega t) + 0.34 \cdot \sin(7 \cdot \omega t)$		
$V_b = 10.71 \cdot \sin(\omega t - 120°) + 0.34 \cdot \sin(3 \cdot (\omega t - 120)) +$ $+0.34 \cdot \sin(5 \cdot (\omega t - 120)) + 0.34 \cdot \sin(7 \cdot (\omega t - 120))$		
$V_c = 11.27 \cdot \sin(\omega t + 120°) + 0.34 \cdot \sin(3 \cdot (\omega t + 120)) +$ $+0.34 \cdot \sin(5 \cdot (\omega t + 120)) + 0.34 \cdot \sin(7 \cdot (\omega t + 120))$		

Line impedances		$Z[m\Omega]$
From	To	
N_0	N_1	$460+j1850$
N_1, N_2, N_5, N_6	N_2, N_5, N_6, N_7	$7.0+j9.7$
N_2, N_3, N_7	N_3, N_4, N_8	$48.3+j10.3$
N_5, N_9	N_9, N_{12}	$22.3+j11.4$
N_9, N_{10}	N_{10}, N_{11}	$20.3+j6.9$
N_{12}	N_{13}	$19.1+j9.8$

TABLE III
PARAMETERS OF THE DISTRIBUTED EGS

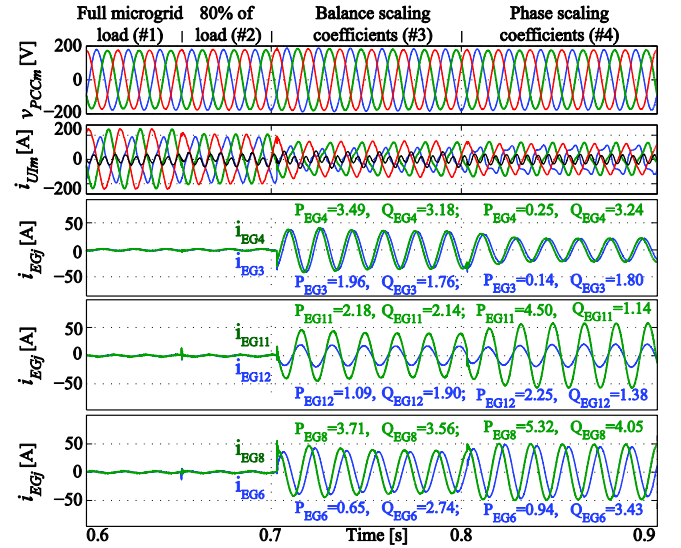| Parameter	EG_j ($N_3, N_4, N_6, N_8, N_{11}, N_{12}$)
Power rating [kVA]	(5.0, 9.0, 7.0, 10.0, 6.0, 5.0)
Overload power rating [kVA]	(5.0, 9.0, 7.0, 10.0, 6.0, 5.0)
Power capacity [kW]	(4.5, 8.0, 1.5, 8.5, 5.0, 2.5)
Max. power capacity [kW]	(4.5, 8.0, 1.5, 8.5, 5.0, 2.5)
Min. power capacity [kW]	(0, 0, 0, 0, 0, 0)

Fig. 4. From top to bottom: PCC voltages, UI currents, and EGs per phase currents and steady state power terms [(kW), (kVA)].

power-based control independently for each phase, which is equivalent to perform independent power sharing per phase. In particular, on the basis of P^*_{PCCm} and Q^*_{PCCm} in (14), the power flow at the PCC can be regulated among the microgrid's phases. Note that as only power quantities are handled, the proposed strategy can be applied to distributed units regardless of their connection scheme.

VI. APPLICATION EXAMPLE

As an application example of the proposed control technique the circuit of Fig. 1 is now considered. The schematic represents a real three-phase four-wire metropolitan distribution power system with aerial wiring currently installed in Brazil. The system was implemented in PSIM software, in order to evaluate the proposed control approach in various operating conditions with time-domain simulations. For simplicity, DERs are modeled as ideal current sources driven by the power commands from the MC, thus neglecting the (irrelevant) influence of the fast current control loops in the analysis of the proposed control technique. The power-based control dynamics was analyzed in [16], which has shown that DERs with different response dynamics do not derail the proposed method.

The utility grid is connected at the node N_0 (*slack node*) and behaves as an ideal voltage source with nominal voltage equal to 13.8 kV line-to-line, 60 Hz. The microgrid is connected to the mains at node N_1, which represents the microgrid PCC, and presents a nominal power of 60 kVA. The values of the considered non-homogeneous network impedances are shown in Table II. The EG parameters are shown in Table III.

A. Comparison Between Phase-Dependent and Phase-Independent Control Strategies

In this section, two different control strategies to calculate the power contributions from EGs are considered and compared in islanded operating mode. With the first strategy, called *phase-independent strategy*, EGs provide the total microgrid's power needs in proportion to their local power availability—measured according to the power-based control

principles [16]—and, notably, in an *independent* way with respect to the particular phase at which EGs are connected. With the second strategy, called *phase-dependent strategy*, the EGs connected to a particular phase contribute to the power needs of the same phase in proportion to their power availability (i.e., EG contributions are proportional to their power availability only if considered *per phase*, as discussed in Section IV). In this latter case, the power needs of each phase are calculated as described in Section V-A, in order to attain a balanced system seen at PCC. This corresponds to perform an independent power sharing in each phase.

To the purpose of highlighting the effects of both compensation strategies, the sequence of operating conditions represented in Fig. 4 is now considered. In particular, interval #1 and #2 pertain to the operation of the system with EGs disabled, whereas intervals #3 and #4 pertain to the operation of the system with EGs driven by the power-based control according to, respectively, the phase-independent and the phase-dependent strategies.

Considering Fig. 4, before 0.7 s, 100 % (interval #1) and 80 % (interval #2) of the nominal microgrid load is connected, with the EGs inactive and the loads fed by the UI during *islanded operation*. Observe that, in spite of the distorted and unbalanced loads, the UI acts as a grid-forming device, and keeps nearly sinusoidal and symmetrical voltages at PCC, with nearly 2 % of total harmonic distortion. The load characteristics are quantitatively reported in Table IV by

TABLE IV
CPT'S POWER TERMS AT PCC AND SCALING
COEFFICIENTS OF FIG. 4

Parameters	(#1)	(#2)	(#3)	(#4)
A_{PCC} [kVA]	56.5	46.9	33.1	32.2
P_{PCC} [kW]	50.6	43.1	31.5	31.5
Q_{PCC} [kVAr]	20.9	16.5	1.1	1.2
N_{PCC} [kVA]	12.2	5.7	**7.8**	**0.5**
D_{PCC} [kVA]	6.5	6.2	6.2	6.3
α_{Pa}	---	---	1.438	1.031
α_{Pb}	---	---	1.438	1.902
α_{Pc}	---	---	1.438	1.627
α_{Qa}	---	---	0.396	0.362
α_{Qb}	---	---	0.396	0.298
α_{Qc}	---	---	0.396	0.498
P_{Gt} [kW]	---	---	13.1	13.4
Losses [kW]	2.49	1.76	0.92	0.92

TABLE V
RMS VALUES OF THE PCC AND MICROGRID VOLTAGES OF FIG. 4

Voltages [V]	(#1)	(#2)	(#3)	(#4)
V_{aN1}	124.5	124.9	126.8	125.3
V_{bN1}	121.9	125.3	124.5	125.6
V_{cN1}	122.6	125.3	125.5	125.5
ΔV_{N1} [%]	**2.1**	**0.3**	**1.8**	**0.2**
V_{N3}	118.9	119.5	125.0	121.7
V_{N4}	119.9	120.5	125.0	122.2
V_{N6}	115.5	119.8	122.7	123.5
V_{N8}	118.1	122.2	123.9	124.3
V_{N11}	116.2	120.4	121.9	123.1
V_{N10}	114.9	119.7	121.8	123.6
ΔV_{MG} [%]	4.2	2.2	2.6	2.1

means of CPT's power terms (described in Section III), while the voltage characteristics are reported in Table V.

After 0.7 s, the results obtained with the *phase-independent* (#3) and the *phase-dependent* (#4) strategies with 80 % of nominal microgrid load are shown. From Fig. 4, Table III and Table IV, we notice that the *phase-independent strategy* drives all EGs to a proportional power contribution with respect to the entire microgrid. However, it fails to reduce the unbalance power (N_{PCC} = 7.8 kVA), which, instead, gets even worse due to the non-uniform active power generation by the EGs in the various phases. This imbalance can also be observed in Table V, by means of the *voltage discrepancy factor* (i.e., ratio between the highest and the lowest voltage values – ΔV). In addition, from Table IV, we notice that the system losses decrease ($\approx$ 48 % of decrease) because the power generation becomes closer to the load [23]. On the other hand, the *phase-dependent strategy* compensates the unbalance power (N_{PCC} = 0.5 kVA) by adjusting individual load power sharing among the phases, while maintaining a proportional power contribution among EGs connected to the same phase. Besides, the amount of delivered active power from EGs is slightly higher (P_{Gt} = 13.4 kW) than the previous case (P_{Gt} = 13.1 kW), because the overall microgrid voltage profile increases (see Table V) at the terminals of the loads, which are modeled as *constant impedances*. Hence, the *phase-dependent strategy* has enhanced the power quality at

the PCC, reduced the power losses, and improved the voltage profile (ΔV_{N1} = 0.2).

From Table IV, we note that the distribution losses obtained with the two strategies is the same. This value of losses corresponds to a quasi-optimum system operation, since reactive and unbalance currents nearly vanish, and the active power properly shares among EGs. The UI supplies only the needed active power, $P_{UIa} = P_{UIb} = P_{UIc}$ = 10.5 kW, and harmonic currents (D_{PCC} = 6.3 kVA), which usually involves relatively low power.

Analyzing Table V, we remark an overall power-quality improvement achieved by applying the power based control. The improvements are higher at the PCC than at any other node of the microgrid, notably, the control has improved the PCC discrepancy factor (ΔV_{N1}) more than the discrepancy factor calculated over the microgrid (ΔV_{MG}).

B. Different Microgrid Operating Modes Under Distorted and Asymmetrical Voltages

With the aim to show the control effectiveness in compensating reactive and unbalance currents and highlight the role of the UI under deteriorated grid voltage (see Table II) a simulation comprising different operating modes and disturbances has been performed. The results are reported in Fig. 5 and Fig. 6.

Instant *t0* corresponds to the last instant of the previously described Fig. 4. At *t1* the mains are restored. Between *t1* and *t2*, the UI synchronizes with the mains and prepares the transition of the microgrid to the grid-connected operation, which is established in *t2*. After the connection instant, the total grid current reference is varied gradually from zero to its final set point value (P^*_{Gridm} = 2.5 kW). The connection procedure occurs smoothly and without resonances—potentially triggered by the distorted grid voltages—thus indicating an adequate control of the UI. The transition is completed at *t3*, then the microgrid keeps a steady state until *t4*. In this interval (*t3 - t4*), the UI currents (i_{UIm}) contain only active and harmonic terms, because all reactive and unbalance currents are compensated by the EGs. At *t4*, the nominal microgrid load is switched on; the steady state is restored within three cycles. In this situation, some coefficients, namely, α_{Pb} and α_{Pc}, reach their maximum value, because the microgrid demand exceeds the per-phase power capacity, which is highlighted in Fig. 6. As discussed in Section IV, the full unbalance power compensation, clearly, cannot be accomplished by the sole contribution of the EGs if their available power is not sufficient to fulfill the needs of the loads; in this case the UI, behaving as an active filter, provides for the remaining unbalance currents (see i_{UIm} in Fig. 5). Of course, after some time, some loads or P^*_{Grid} might be readjusted.

Note that, even in this last case, the grid current waveforms (i_{Gm}) become proportional to the phase voltages (v_{Gm}), performing a *resistive load synthesis* compensation strategy [24]. That results in unity power factor at PCC, and complies with the definition of balanced system, in which $G_m = G^b$ and $B_m = B^b$ to all frequencies.
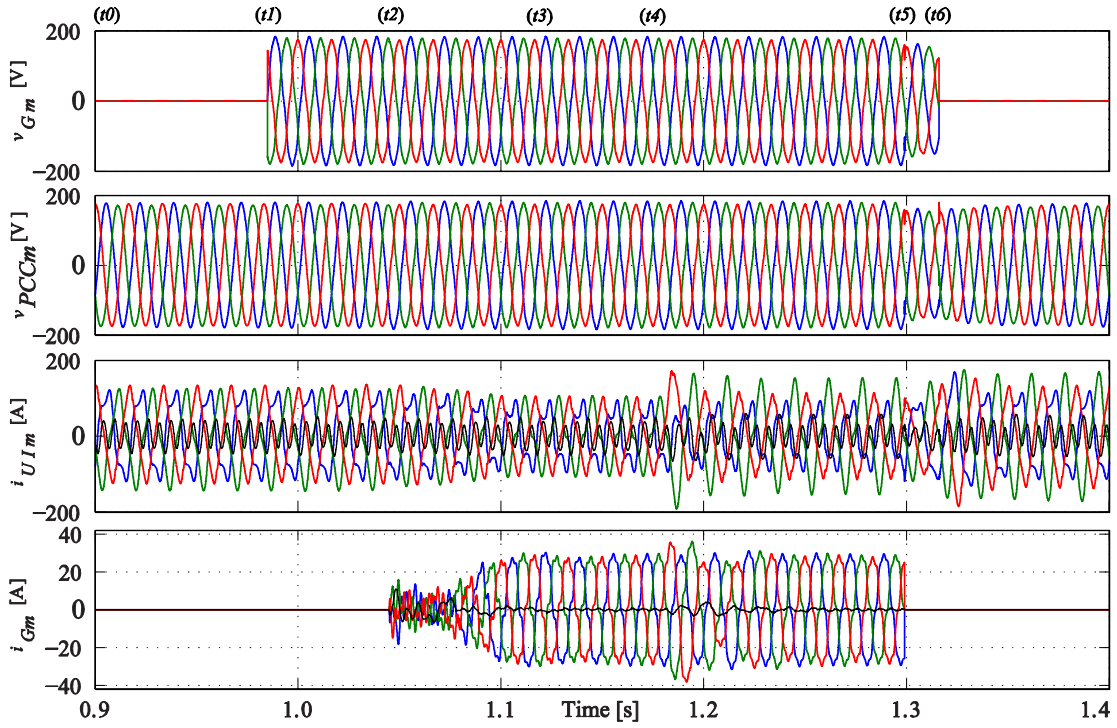
Fig. 5.   Obtained results in case of distorted and asymmetrical voltages. From top to bottom: grid and PCC voltages, UI and grid currents.
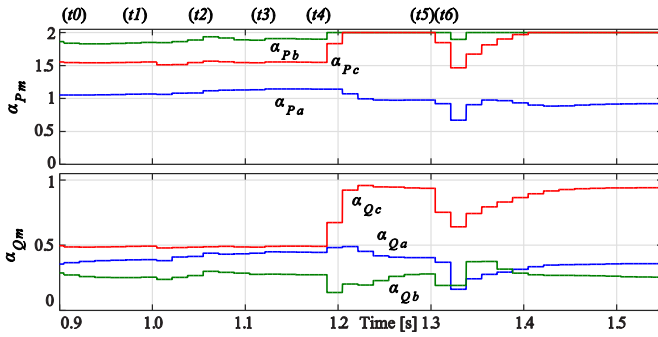

Fig. 6.   Phase scaling coefficients related to Fig. 5.

Finally, at instant *t5*, the mains is suddenly disconnected, causing a non-intentional transition to the islanded operation. The MC processes and eventually detects the islanded condition during the interval between instants *t5* and *t6*; successively, UI becomes the grid-forming voltage source of the islanded microgrid. Across the transition to the non-intentional island, we notice a small transient consisting in voltage sag occurring during the islanding detection interval, which is promptly cleared when the islanded operation is detected (see v_{PCCm}, Fig. 5). Despite of that, the system reaction is prompt and smooth. After *t6*, the system operates again in stand-alone, with the power-based control enabled. This means that UI provides only a portion of the load currents, while the remaining part is requested to distributed EGs. We highlight that even under islanded operation at full load, the reactive and unbalanced reactive current terms are fully compensated by the EGs, indeed, coefficients α_{Qm} do not saturate, as can be noticed by inspecting the last instants of the simulation given in Fig. 6.
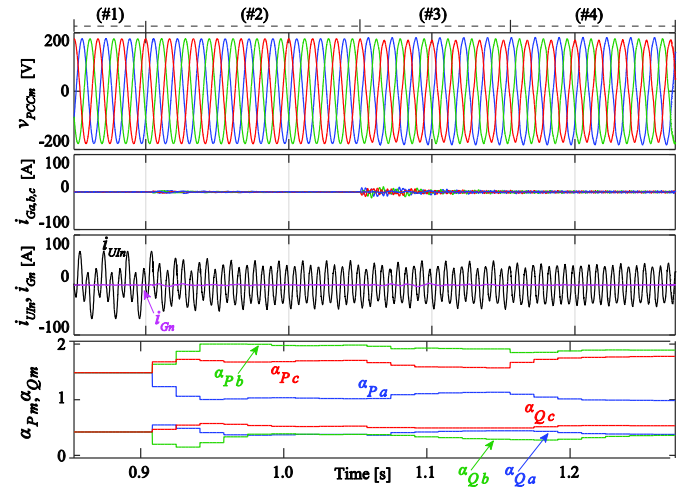

Fig. 7.   From top to bottom: PCC voltages, grid currents for phases *a*, *b* and *c*, neutral currents in the UI and grid, and phase scaling coefficients (per phase).

C. Homopolar Current Compensation

To discuss the homopolar current compensation by arbitrary connected DERs, the cases #1, #2, #3 of Fig. 7 are considered. In case #1, the microgrid is connected to an ideal grid with zero current exchange (P^*_{Gridm}, $Q^*_{Gridm} = 0$) under *phase-independent strategy* (to be similar to the islanded mode of case (#3) in Fig. 4). Then, in case #2, the control strategy is changed to *phase-dependent*, as in case (#4) of Fig. 4, and one can notice that the fundamental component of the UI's neutral current (i.e., homopolar current) is significantly reduced, as quantitatively shown in Table VI.

	cases	#1	#2	#3	#4
UI's neutral	**Fund. [A]**	28.47	4.26	10.79	3.60
current	**3rd Harm. [A]**	41.20	41.10	39.38	39.59

In case #3, the PCC voltages are distorted and asymmetrical, which increases the circulation of homopolar currents. Such currents cannot be compensated by the EGs, because the proposed method is based on conductance and reactivity load quantities, performing a *resistive load synthesis* compensation strategy [24], as discussed in Sections III and IV. Indeed, the homopolar currents are naturally compensated only by the line-to-neutral connected inverters, since the line-to-line inverters are decoupled from neutral conductor, as discussed in Section II.

D. Power Flow Control Among Different Phases

Case #4 of Fig. 7 evaluates the coordinated control of power flow exchange among the microgrid's phases. Supposing the condition that phase *a* drains active power (e.g., to charge its energy storage devices) the MC can adjust the power sharing among the phases and control the power flow from phases *b* and/or *c* to phase *a*. To this end, the references P^*_{PCCm} of (14) and (15) are set to $P^*_{PCCa} = P^*_{PCCb} = 11$ kW and $P^*_{PCCc} = 9.5$ kW, corresponding to the phase power supplied by the UI, because of P^*_{Gridm}, $Q^*_{Gridm} = 0$ in (15). Then, the phase scaling coefficients assume the following values in steady state $(\alpha_{Pa}, \alpha_{Pb}, \alpha_{Pc}) = (0.841, 1.901, 1.865)$ and $(\alpha_{Qa}, \alpha_{Qb}, \alpha_{Qc}) = (0.293, 0.444, 0.538)$, which corresponds to $(P_{Gat}, P_{Gbt}, P_{Gct}) = (-2.00, 6.75, 8.65)$ kW and $P_{Gt} = 13.4$ kW. These previous coefficient values compared to those in Table IV show that the EGs connected to phase *c* increase their power generation ($\alpha_{Pc} = 1.627 \rightarrow 1.865$), while the EGs of phase *a* store energy ($\alpha_{Pa} = 1.031 \rightarrow 0.841$). In Fig. 7, despite of the fact that the UI provides phase unbalance power $(P_{UIa}, P_{UIb}, P_{UIc}) = (11.0, 11.0, 9.5)$ kW, the grid currents remain balanced, notably; the power flow through PCC is practically null (see $i_{Ga,b,c}$, in Fig. 7). We remark that the UI and the EGs provides the same amount of power, as previously discussed in Section VI-A for case (#4), $P_{Gt} = 13.4$ kW.

VII. CONCLUSION

This paper proposes a new control technique to coordinate the power flow among phases of a three-phase four-wire low-voltage microgrid with arbitrarily connected single-phase inverters. The technique works properly even under weak-grid conditions (distorted and asymmetrical voltages), and ensures optimum power sharing among phases so as to compensate reactive and unbalance current terms. It enhances the microgrid flexibility and reliability, and achieves unity power factor at PCC. Moreover, it keeps small the voltage deviations at grid nodes and minimizes the distribution losses.

The proposed control is applicable to four-wire microgrids, irrespective of topology, inverter connection codes, and line impedances. Moreover, even the harmonic and homopolar currents can be eliminated by a proper control of line-to-neutral connected inverters and, in grid-connected operation, by the utility interface.

As the coordinated control makes use of conservative power terms, it keeps good performance and stability even under deteriorated grid voltages. In terms of implementation, the proposed control requires a reliable, but non-time-critical, communication link between the master controller and the distributed slave units.

Using the proposed technique, future works will cope with the coordinated and simultaneous operation of balanced three-phase and single-phase inverters, as well as the case of any inverter operating on voltage source mode. Further, the case of three-wire microgrids is also going to be dealt with.

REFERENCES

[1] J. J. Conti *et al.*, "Annual energy outlook 2014—With projections to 2040," U.S. Dept. Energy, U.S. Energy Inf. Admin., Washington, DC, USA, Tech. Rep. DOE/EIA-0383(2014), 2014.

[2] D. E. Olivares *et al.*, "Trends in microgrid control," *IEEE Trans. Smart Grid*, vol. 5, no. 4, pp. 1905–1919, Jun. 2014.

[3] A. Khodaei, "Provisional microgrids," *IEEE Trans. Smart Grid*, vol. 6, no. 3, pp. 1107–1115, May 2015.

[4] Z. Wang, B. Chen, J. Wang, M. M. Begovic, and C. Chen, "Coordinated energy management of networked microgrids in distribution systems," *IEEE Trans. Smart Grid*, vol. 6, no. 1, pp. 45–53, Jan. 2015.

[5] Q. Sun, J. Zhou, J. M. Guerrero, and H. Zhang, "Hybrid three-phase/single-phase microgrid architecture with power management capabilities," *IEEE Trans. Power Electron.*, vol. 30, no. 10, pp. 5964–5977, Oct. 2015.

[6] S. Bala, *Integration of Single-Phase Microgrids*, 1st ed. Ann Arbor, MI, USA: ProQuest, 2008.

[7] *AC Power Source Summary*. Accessed on Jul. 5, 2016. [Online]. Available: www.hyvac.com/tech_support/electrical_sources_worldwide.pdf

[8] M. Hamzeh, H. Karimi, and H. Mokhtari, "Harmonic and negative-sequence current control in an islanded multi-bus MV microgrid," *IEEE Trans. Smart Grid*, vol. 5, no. 1, pp. 167–176, Jan. 2014.

[9] A. Ghosh and A. Joshi, "A new approach to load balancing and power factor correction in power distribution system," *IEEE Trans. Power Del.*, vol. 15, no. 1, pp. 417–422, Jan. 2000.

[10] A. Maknouninejad and Z. Qu, "Realizing unified microgrid voltage profile and loss minimization: A cooperative distributed optimization and control approach," *IEEE Trans. Smart Grid*, vol. 5, no. 4, pp. 1621–1630, Jul. 2014.

[11] P.-T. Cheng, C.-A. Chen, T.-L. Lee, and S.-Y. Kuo, "A cooperative imbalance compensation method for distributed-generation interface converters," *IEEE Trans. Ind. Appl.*, vol. 45, no. 2, pp. 805–815, Mar./Apr. 2009.

[12] M. Savaghebi, A. Jalilian, J. C. Vasquez, and J. M. Guerrero, "Autonomous voltage unbalance compensation in an islanded droop-controlled microgrid," *IEEE Trans. Ind. Electron.*, vol. 60, no. 4, pp. 1390–1402, Apr. 2013.

[13] T. Caldognetto, P. Tenti, P. Mattavelli, S. Buso, and D. I. Brandao, "Cooperative compensation of unwanted current terms in low-voltage microgrids by distributed power-based control," in *Proc. Brazil. Power Electron. Conf. (COBEP-SPEC)*, Fortaleza, Brazil, 2015, pp. 1–7.

[14] Z. Liu and J. Liu, "Indirect current control based seamless transfer of three-phase inverter in distributed generation," *IEEE Trans. Power Electron.*, vol. 29, no. 7, pp. 3368–3383, Jul. 2014.

[15] S. Yoon, H. Oh, and S. Choi, "Controller design and implementation of indirect current control based utility-interactive inverter system," *IEEE Trans. Power Electron.*, vol. 28, no. 1, pp. 26–30, Jan. 2013.

[16] T. Caldognetto, S. Buso, P. Tenti, and D. I. Brandao, "Power-based control of low-voltage microgrids," *IEEE J. Emerg. Sel. Topics Power Electron.*, vol. 3, no. 4, pp. 1056–1066, Dec. 2015.

[17] A. Bidram and A. Davoudi, "Hierarchical structure of microgrids control system," *IEEE Trans. Smart Grid*, vol. 3, no. 4, pp. 1963–1976, Dec. 2012.

[18] Y. Yang, F. Blaabjerg, and H. Wang, "Constant power generation of photovoltaic systems considering the distributed grid capacity," in *Proc. IEEE Appl. Power Electron. Conf. Expo.*, Fort Worth, TX, USA, 2014, pp. 379–385.

[19] P. Tenti, H. K. M. Paredes, and P. Mattavelli, "Conservative power theory, a framework to approach control and accountability issues in smart microgrids," *IEEE Trans. Power Electron.*, vol. 26, no. 3, pp. 664–673, Mar. 2011.

[20] A. Costabeber, P. Tenti, T. Caldognetto, and E. V. Liberado, "Selective compensation of reactive, unbalance, and distortion power in smart grids by synergistic control of distributed switching power interfaces," in *Proc. Eur. Conf. Power Electron. Appl.*, Lille, France, 2013, pp. 1–9.

[21] J.-Y. Kim, S.-K. Kim, and J.-H. Jeon, "Coordinated state-of-charge control strategy for microgrid during islanded operation," in *Proc. IEEE Int. Symp. Power Electron. Distrib. Gener. Syst.*, Aalborg, Denmark, 2012, pp. 133–139.

[22] A. Ahmed, L. Ran, S. Moon, and J.-H. Park, "A fast PV power tracking control algorithm with reduced power mode," *IEEE Trans. Energy Convers.*, vol. 28, no. 3, pp. 565–575, Sep. 2013.

[23] T. Caldognetto, P. Tenti, A. Costabeber, and P. Mattavelli, "Improving microgrid performance by cooperative control of distributed energy sources," *IEEE Trans. Ind. Appl.*, vol. 50, no. 6, pp. 3921–3930, Nov./Dec. 2014.

[24] T. E. Nunez-Zuniga and J. A. Pomilio, "Shunt active power filter synthesizing resistive load," *IEEE Trans. Power Electron.*, vol. 17, no. 2, pp. 273–278, Mar. 2002.

Marcelo G. Simões (F'16) received the B.Sc. and M.Sc. degrees from the University of São Paulo, Brazil, in 1985 and 1990, respectively, the Ph.D. degree from the University of Tennessee, USA, in 1995, and the D.Sc. degree (Livre-Docência) from the University of São Paulo, in 1998. He was an U.S. Fulbright Fellow with the Institute of Energy Technology, Aalborg University, Denmark, from 2014 to 2015. He is a Pioneer to apply neural networks and fuzzy logic in power electronics, motor drives and renewable energy systems. His fuzzy logic-based modeling and control for wind turbine optimization is used as a basis for advanced wind turbine control and it has been cited worldwide. His leadership in modeling fuel cells is internationally and highly influential in providing a basis for further developments in fuel cell automation control in many engineering applications. He made substantial and lasting contribution of artificial intelligence technology in many applications, power electronics and motor drives, fuzzy control of wind generation system, such as fuzzy logic-based waveform estimation for power quality, neural network-based estimation for vector controlled motor drives, and integration of alternative energy systems to the electric grid through AI modeling based power electronics control.

Danilo I. Brandao (S'14–M'16) received the Ph.D. degree in electrical engineering from the University of Campinas, Brazil, in 2015. He was a Visiting Researcher with the Colorado School of Mines, USA, in 2009 and 2013. He was a visiting Ph.D. student with the University of Padova, Italy, in 2014. He is currently a Professor with the Department of Electrical Engineering, Federal University of Minas Gerais, Brazil. His main research interests include active power filter, power quality, distributed compensation strategies, and microgrids.

Tommaso Caldognetto (S'10–M'16) received the M.S. (Hons.) degree in electronic engineering and the Ph.D. degree in information engineering from the University of Padova, Italy, in 2012 and 2016, respectively. In 2014, he was a visiting Ph.D. student with the Institute for Automation of Complex Power Systems, University of Aachen, Germany. He is currently a Post-Doctoral Research Fellow with the Department of Technology and Management, University of Padova. His research interests include control of grid-tied converters, microgrid architectures, and real-time simulation for power electronics.

José A. Pomilio (M'92–SM'02) was born in Jundiaí Brazil, in 1960. He received the B.S., M.S., and Ph.D. degrees in electrical engineering from the University of Campinas, Brazil, in 1983, 1986, and 1991, respectively. From 1988 to 1991, he was the Head of the Power Electronics Group, Brazilian Synchrotron Light Laboratory. He was a Visiting Professor with the University of Padova, Italy, in 1993 and 2015, and with the Third University of Rome, Italy, in 2003. He is a Professor with the School of Electrical and Computer Engineering, University of Campinas, where he has been teaching since 1984. His main interests are power electronics and power quality. He was the President of the Brazilian Power Electronics Society from 2000 to 2002, and a member of the Administrative Committee of the IEEE Power Electronics Society from 1997 to 2002. He is currently an Associate Editor of the IEEE TRANSACTIONS ON POWER ELECTRONICS.

Fernando P. Marafão (S'95–M'05) received the B.S. degree in electrical engineering from Universidade Estadual Paulista (UNESP), Sorocaba, Brazil, in 1998, and the M.Sc. and Ph.D. degrees from the University of Campinas, Brazil, in 2000 and 2004, respectively. In 2002, he joined the Power Electronics Group, University of Padova, Italy, as a visiting student on digital control techniques for active power filters. In 2013, he joined the ACEPS Group, Colorado School of Mines, USA, as a Visiting Scholar on Autonomous and Intelligent Distributed Energy Systems. Since 2005, he has been with UNESP, being an Associate Professor with the Group of Automation and Integrating Systems. His current research interests include power definitions under nonsinusoidal and unbalanced conditions, accountability, revenue metering and digital processing techniques for power electronics, and smart grid applications. He is a member of the Brazilian Power Electronics Society and Brazilian Automatic Society.

Paolo Tenti (F'99) is a Professor of Electronics and Power Electronics with the Department of Information Engineering, University of Padova, Italy. From 2001 to 2008, he was the Director of the Department of Information Engineering, University of Padova, where he served as the Chairman of the Council of Department Directors, from 2003 to 2008. His main research interests are in power electronics and industrial electronics. His work currently deals with power quality, distributed compensation techniques, and smart micro-grids. He was a recipient of the IEEE Millennium Medal in 2000. From 1991 to 2001, he was a member of the Executive Board of the IEEE Industry Applications Society, and in 1997, he served as an IAS President. Since 1996, he has been the President of CREIVen, Research Center on Industrial Electronics, Padova, Italy.